Hindawi Publishing Corporation
Journal of Nanomaterials
Volume 2013, Article ID 702679, 8 pages
http://dx.doi.org/10.1155/2013/702679

Research Article

Synthesis of h- and α-MoO_3 by Refluxing and Calcination Combination: Phase and Morphology Transformation, Photocatalysis, and Photosensitization

Pannipa Wongkrua,[1] Titipun Thongtem,[1] and Somchai Thongtem[2,3,4]

[1] *Department of Chemistry and Center for Innovation in Chemistry, Faculty of Science, Chiang Mai University, Chiang Mai 50200, Thailand*
[2] *Department of Physics and Materials Science, Faculty of Science, Chiang Mai University, Chiang Mai 50200, Thailand*
[3] *Materials Science Research Center, Faculty of Science, Chiang Mai University, Chiang Mai 50200, Thailand*
[4] *Science and Technology Research Institute, Chiang Mai University, Chiang Mai 50200, Thailand*

Correspondence should be addressed to Titipun Thongtem; ttpthongtem@yahoo.com
and Somchai Thongtem; schthongtem@yahoo.com

Received 29 April 2013; Accepted 18 June 2013

Academic Editor: Chunyi Zhi

Hexagonal molybdenum oxide (h-MoO_3) nano- and microrods were successfully synthesized by refluxing of $(NH_4)_6Mo_7O_{24}{\cdot}4H_2O$ solutions with the pH 1 at 90°C for 1, 3, 5, and 7 h and were further transformed into orthorhombic molybdenum oxide (α-MoO_3) microplates by calcination at 450°C for 6 h. These selected products were used to determine the degradation of methylene blue dye under 35 W xenon lamp for 0–180 min, due to the photocatalysis and photosensitization processes. In this research, catalytic activity of the metastable h-MoO_3 has higher efficiency than that of the thermodynamically stable α-MoO_3. Their phase and morphology transformation was also explained according to the experimental results.

1. Introduction

MoO_3 is one of the transition metal oxide materials. It has a wide range of applications such as imaging devices, smart windows, electrodes of rechargeable batteries, gas sensors, and supported catalysts [1]. Since MoO_3 is a 3.15 eV wide band gap n-type semiconductor, it is well known as one of the most widely used photocatalysts. Its catalytic efficiency has long been known, for example, in alcohol and methane [2, 3]. Its crystalline structures are known to have three common polymorphs: one thermodynamically stable orthorhombic MoO_3 (α-MoO_3) and two metastable phases hexagonal MoO_3 (h-MoO_3) and monoclinic MoO_3 (β-MoO_3). The MoO_6 octahedrons are the basic building units of all MoO_3 structures. For α-MoO_3, the MoO_6 octahedrons share edges and corners, resulting in zigzag chains and a unique layer structure. But for β-MoO_3, it has a ReO_3-related structure, in which the MoO_6 octahedrons share corners to form distorted cubes. The h-MoO_3 is also composed of the same zigzag chains of MoO_6 octahedrons connecting through the cis-positions [1, 4]. Moreover, h-MoO_3 exhibits phase stability up to 436°C at which the irreversible phase transition occurs to form orthorhombic α-MoO_3 [5]. Various molybdenum oxide structures and morphologies have been synthesized by different methods: hexagonal rod-like h-MoO_3 by liquid phase deposition [1], nanospheres by ultrasonic-assisted synthesis [3], hexagonal rod-like h-MoO_3 by precipitation [4, 6], MoO_3 nanorods by ultrasonic synthesis [5, 7], α-MoO_3 nanobelts by hydrothermal synthesis [8, 9], h-MoO_3 rods by solution precipitation and solvothermal treatment [10], MoO_3 nanostructures by solution combustion [11], α-MoO_3 polycrystalline thin films by spray pyrolysis [12], MoO_3 nanobelts by hydrothermal method [13, 14], h-MoO_3 and α-MoO_3 nanoparticles by hydrothermal synthesis [15], h-MoO_3

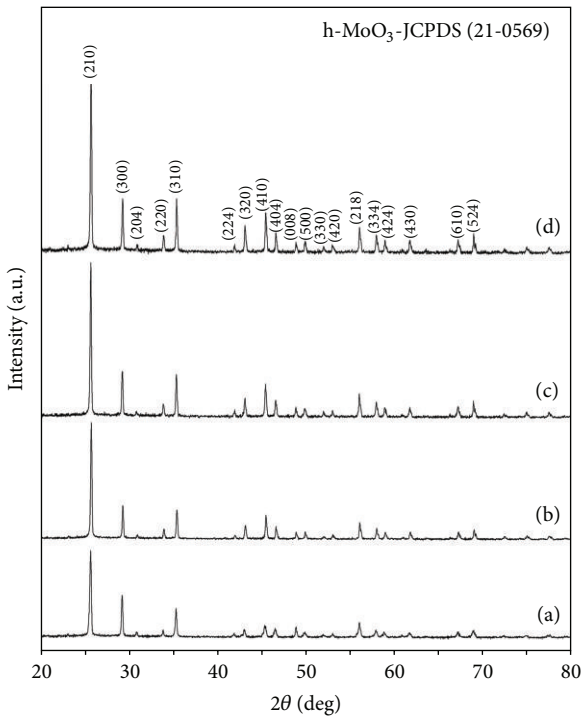

Figure 1: XRD patterns of h-MoO_3 synthesized by refluxing method for ((a)–(d)) 1, 3, 5, and 7 h, respectively.

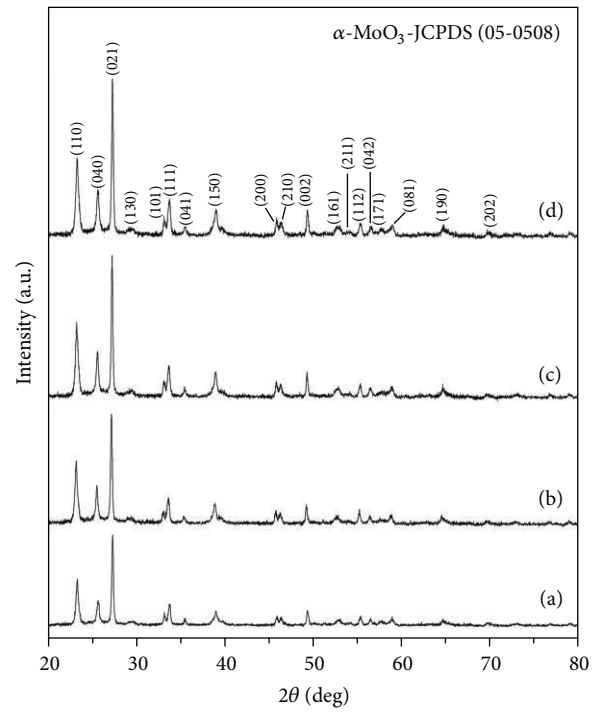

Figure 2: XRD patterns of α-MoO_3 synthesized by refluxing method for ((a)–(d)) 1, 3, 5, and 7 h and followed by calcination at 450°C for 6 h, respectively.

nanorods by precipitation [16, 17], α-MoO_3 microplates by microwave plasma process [18], and α-MoO_3 nanocrystals by oil bath heating and sintering combination [19].

In this research, both hexagonal and orthorhombic molybdenum oxide phases were synthesized by refluxing process to form the first and followed by high temperature calcination to form the second. Different phases, phase and morphology transformation (PMT), degradation of methylene blue dye, and mechanisms of photocatalysis and photosensitization are also discussed.

2. Experimental Procedures

To synthesize h-MoO_3 and α-MoO_3 with different morphologies, 0.005 mole ammonium heptamolybdate tetrahydrate ($(NH_4)_6Mo_7O_{24}{\cdot}4H_2O$) was dissolved in 40 mL of deionized water with continuous stirring at room temperature for 30 min. Subsequently, 2 M HNO_3 was added to the solution until achieving the pH 1 and forming of the clear solution. The solution was processed by a refluxing method at 90°C for 1, 3, 5, and 7 h. In the end, light-blue precipitates were synthesized, separated by filtration, washed, and dried in an electric oven at 80°C for 24 h. The products were further calcined at 450°C for 6 h to form powders.

Crystalline phases, morphologies, and vibration modes were characterized by a Philips X'Pert MPD X-ray diffractometer (XRD) at 45 kV and 35 mA with Cu K_α radiation in the 2θ range of 20–80 deg with a scanning rate of 0.04 deg per step, a JEOL JSM-6335F scanning electron microscope (SEM) with an accelerating voltage of 15 kV across the LaB_6 cathode,

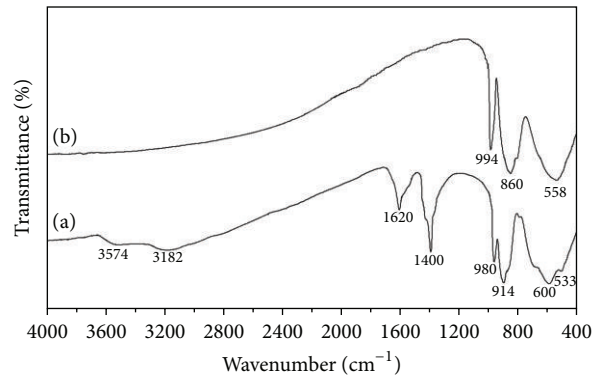

Figure 3: FTIR spectra of (a) h-MoO_3 and (b) α-MoO_3.

a JEOL JEM-2100F transmission electron microscope (TEM) and selected area electron diffraction (SAED) at 200 kV, and a Bruker Tensor 27 Fourier transform infrared (FTIR) spectrometer with KBr as a diluting agent operated in the range of 4000–400 cm^{-1} with the resolution of 4 cm^{-1}. In the end, photoluminescence (PL) of the products was analyzed by a LS50B PerkinElmer fluorescence spectrometer using 337 nm excitation wavelength at room temperature and photoabsorption by a Lambda-25 PerkinElmer UV-visible spectrometer in the wavelength range of 250–800 nm.

The degradation of methylene blue (MB) dye aqueous solutions was investigated. Each 150 mg MoO_3 was added to a 150 mL 1.0×10^{-5} M MB solution, which was stirred for 30 min in the dark condition to establish an adsorption-desorption

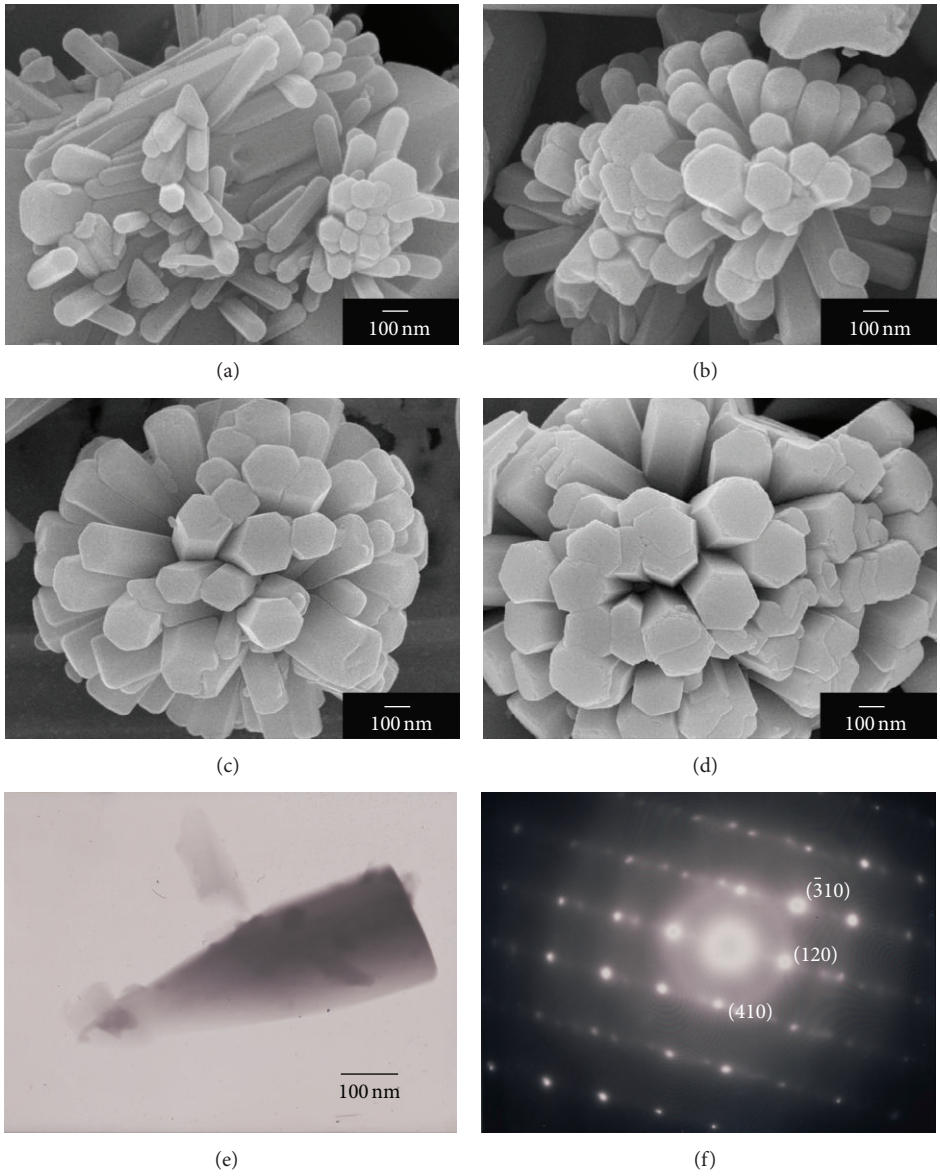

FIGURE 4: SEM images of h-MoO_3 synthesized by refluxing method for ((a)–(d)) 1, 3, 5, and 7 h, respectively. (e) TEM image and (f) SAED pattern of h-MoO_3 processed for 7 h.

equilibrium. Thus, the MB dye molecules have a chance to adsorb on the MoO_3 surfaces. Degradation was initiated by a 35 W Xe lamp for 0–180 min. The absorbance peak (strongest intensity) at 664 nm wavelength, determined by UV-visible spectrometer, was assumed to be linearly dependent on the concentration of MB solution. Decolorization efficiency (%) was calculated by $((I_o - I)/I_o) \times 100$, where I_o and I were the absorbance intensities of the solutions before and after degradation, respectively.

3. Results and Discussion

3.1. XRD. XRD patterns of the products synthesized by a refluxing method for 1, 3, 5, and 7 h are shown in Figure 1. All the diffraction peaks can be indexed to be pure hexagonal (h) MoO_3 phase (JCPDS no. 21-0569) [20]. Their crystalline degrees were improved by increasing the length of reaction time. Upon calcination of the products at 450°C for 6 h in air, they were transformed into the orthorhombic (α) MoO_3 (JCPDS no. 05-0508) [20] (Figure 2) with no impurity detection.

3.2. FTIR. The functional groups of the products with the best crystalline degree were identified by FTIR (Figure 3) over the range of 4000–400 cm^{-1} wavenumber. For h-MoO_3, its spectrum shows peaks at 3574 cm^{-1} and 1620 cm^{-1} corresponding to the stretching and bending vibrations of O–H bonds of adsorbed water molecules, respectively. Those at 3182 cm^{-1} and 1400 cm^{-1} are due to the stretching and bending vibration of N–H of NH_4^+ groups, consistent with

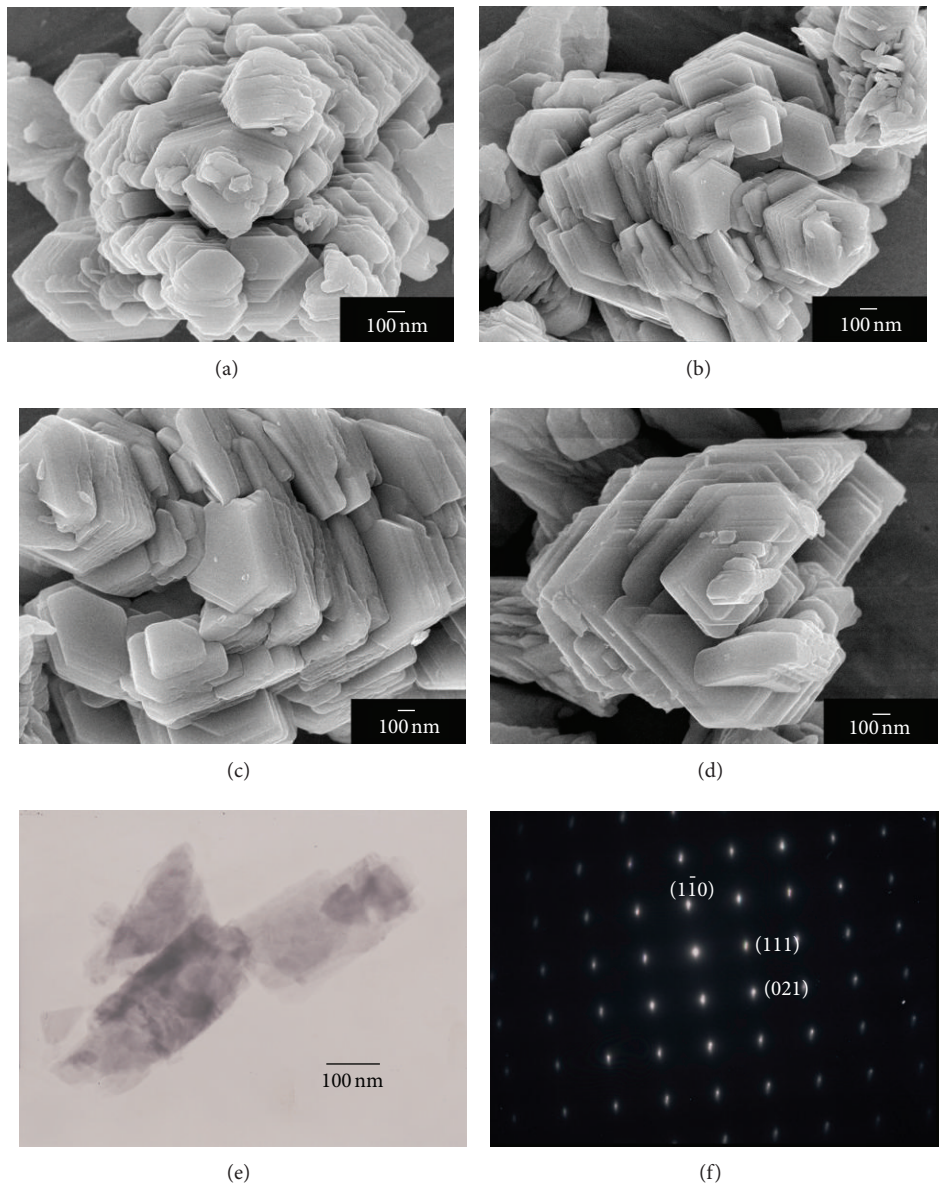

Figure 5: SEM images of α-MoO_3 synthesized by refluxing method for ((a)–(d)) 1, 3, 5, and 7 h and followed by 450°C and 6 h calcination. (e) TEM image and (f) SAED pattern of (d).

the previous report [16]. The 1000–400 cm^{-1} peaks correspond to the stretching and bending vibrations of metal-oxygen characteristic bonds. The peaks at 980 cm^{-1} and 914 cm^{-1} are the characteristic of Mo=O stretching vibrations, including those between 600 and 500 cm^{-1} corresponding to the vibration of Mo–O bonds [15, 17]. But for α-MoO_3, the spectrum shows three strong peaks: 994 cm^{-1} attributed to the terminal M=O stretching vibration with an indicator of the layered orthorhombic MoO_3 phase, 860 cm^{-1} to the stretching mode of oxygen in Mo–O–Mo bonds, and a broad band at 558 cm^{-1} to the bending vibration of oxygen atom linked to three metal atoms [14, 15, 18]. No water was detected in this orthorhombic-structured product.

3.3. EM and PMT. Figures 4(a)–4(e) show SEM and TEM images of h-MoO_3 synthesized by refluxing method for different lengths of reaction time. The products shaped like clusters of hexagonal rods with the most complete at 7 h processing. The rods were 83.82, 143.57, 182.58, and 220.84 nm in diameter for 1, 3, 5, and 7 h processing, respectively. They became enlarged, by transforming from nanosized to microsized rods, with increasing the processing time. In this research, the rods grew out of a center [21], appearing as clusters/flowers of hexagonal rod-like petals and becoming the most complete flowers for 7 h processing. A SAED pattern of h-MoO_3 (Figure 4(f)) reveal as single crystalline h-MoO_3. When these products were calcined at 450°C for 6 h, h-MoO_3 structure ($a = b = 10.5310$ Å, $c = 14.8760$ Å,

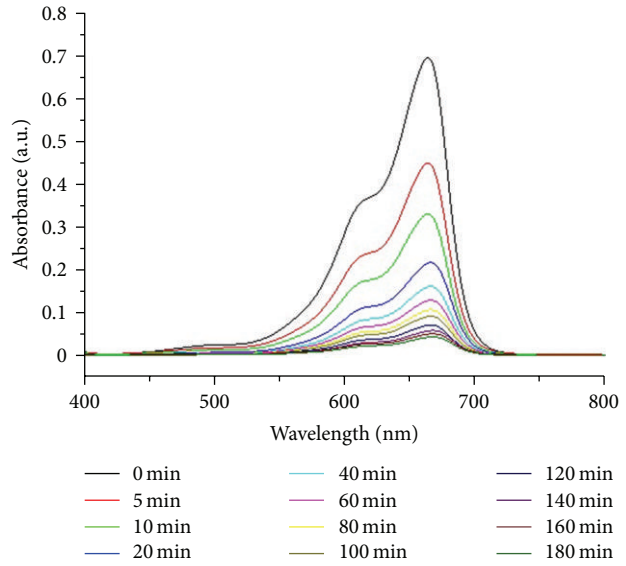

FIGURE 6: UV-visible spectra of MB solution containing α-MoO_3, synthesized by 90°C refluxing for 7 h in combination with 450°C calcination for 6 h and irradiated by xenon light for different lengths of time.

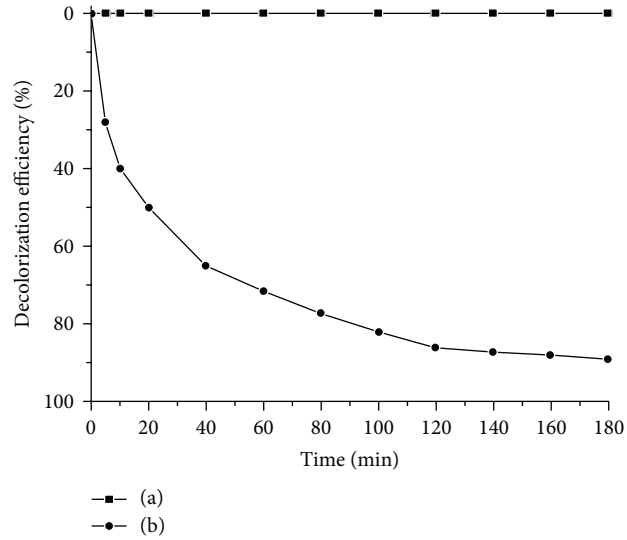

FIGURE 7: Decolorization efficiency of MB: (a) catalyst-free solution and (b) the solution containing α-MoO_3 catalyst synthesized by 90°C refluxing for 7 h in combination with 450°C and 6 h calcination and irradiated by xenon light for different lengths of time.

$\alpha = \beta = 90$ deg, and $\gamma = 120$ deg) [20] transformed into α-MoO_3 ($a = 3.9620$ Å, $b = 13.8580$ Å, $c = 3.6970$ Å, and $\alpha = \beta = \gamma = 90$ deg) [20]. Concurrently, their morphology transformed from flowers of hexagonal rods (Figures 4(a)–4(e)) into assemblies of microplates (Figures 5(a)–5(e)), due to the arrangement of Mo and O atoms to achieve the lowest energy. During 450°C calcination, flowers of h-MoO_3 rod-like petals were separated into a number of rods. All atoms of these individual rods were at high energy, leading to the vibration and diffusion process. The strength of vibration and diffusion of the solid was controlled by the calcination temperature, bond strength, type of bonds, and others. Thus, the rods were no longerable to retain their original morphologies. When the calcination process was complete at 6 h, the solid was cooled down to room temperature. During cooling, the vibration and diffusion of all atoms slowed down. The atoms returned to their new lattice sites which were at the lowest energy. In the end, the atoms formed a orthorhombic crystalline structure (α-MoO_3) of which the unit cells arranged themselves into assemblies of microplates. SAED pattern (Figure 5(f)) of the Figure 5(e) product was indexed to be α-MoO_3 with the [−1 −1 2] direction as zone axis.

In this research, h-MoO_3 flowers with 5 and 7 h refluxing were more perfect than those synthesized by ultrasonic synthesis [7] and chemical precipitation [16, 17], including the corresponding α-MoO_3 microplates which were more systematic than those synthesized by microwave plasma [18].

3.4. Photocatalysis, Photosensitization, and Mechanisms. The MB solution containing metastable h-MoO_3 phase with 7 h refluxing was studied and became colorless by 30 min stirring during establishing adsorption-desorption equilibrium. Possibly, the solution containing h-MoO_3 was exposed to UV radiation.

Photocalytic properties of α-MoO_3 containing methylene blue (MB) solution irradiated by xenon light for 0–180 min (Figure 6) were investigated. For cationic MB dye aqueous solution, there are two absorption bands at 293 nm or 4.23 eV (π–π^*) and 664 nm or 1.87 eV (n–π^*) [19]. In this research, intensities of absorption peaks at 664 nm were decreased with the increase in the lengths of irradiation time. Comparing to the catalyst-free solution, the 180 min degradation of MB solution (Figure 7) containing α-MoO_3 catalyst synthesized by 90°C refluxing for 7 h in combination with 450°C calcination for 6 h was 88%. During photocatalysis or changing of a chemical reaction rate by photons, electrons in valence band of α-MoO_3 were excited and transferred to its conduction band under xenon light radiation, leaving holes in valence band behind. Holes combined with H_2O to form •H and •OH radicals. Concurrently, the electrons in conduction band diffused to the adsorbed O_2 to form activated $\bullet O_2^-$ with subsequent transforming of H_2O molecules into •OH radicals. These oxidative species could mineralize MB dye back into original chemical forms of CO_2 and H_2O creating a cleaner and safer environment [22]. If the processes were not possible, electron-hole pairs would recombine together to generate heat on the materials. Photocatalytic activity was controlled by various factors, including structure, particle size, surface area, crystalline degree, surface-adsorbed water molecules, and hydroxyl groups [23]. The present results show that catalytic activity of the metastable h-MoO_3 phase

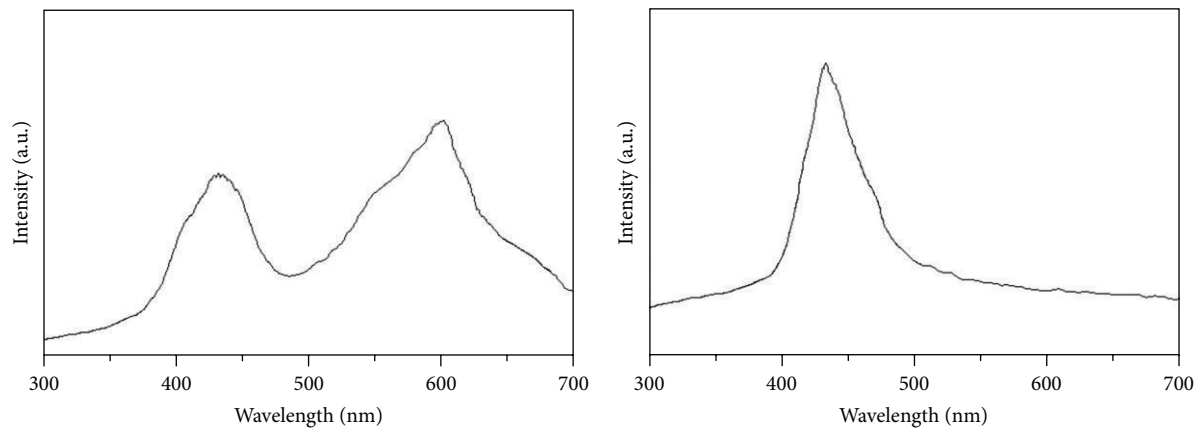

Figure 8: Fluorescence spectra of (a) h-MoO_3 and (b) α-MoO_3.

has higher efficiency than that of the thermodynamically stable α-MoO_3 one.

Photosensitization or the process of initiating reaction by a photonic absorber and transfer of energy to reactants was also possible. Upon irradiation of the solutions by xenon light, the MB dye absorbed photon energy and induced the π–π^* transition (4.23 eV [19]) [14], including n–π^* transition (1.87 eV [19]). The excited electrons of the MB dye diffused to conduction band (d-orbital) of MoO_3 and reacted with adsorbed oxygen to form $\bullet O_2^-$ oxidants which further mineralized the MB dye back into CO_2 and H_2O. Photolysis or chemical decomposition of dye induced by photon relates to its structural stability [14], which leads to the mineralization process.

In summary, decolorization of MB dye was able to proceed by the photocatalysis and photosensitization processes or either of the two, influenced by photonic energy, energy gap of MoO_3 catalyst, gaps of n–π^* and π–π^* states of MB dye, and others.

3.5. PL. Figure 8 shows photoluminescence of h-MoO_3 and α-MoO_3 excited by 337 nm wavelength at room temperature. Photons with energy exceeding their energy gaps reflected on the products and generated photoexcited electrons, which are not stable. Thus, they jumped back to a basic state and emitted fluorescence photons with lower energy. They both show strong emission peaks at 436 nm in accordance with other reports [9, 10, 18, 19], due to the electron-hole recombination. Moreover, h-MoO_3 has another extra peak at 606 nm specified as the presence of adsorbed oxygen on the material [10].

3.6. UV-Visible Absorption. UV-visible absorption spectroscopy has been used to study photonic properties of materials. Experimentally, the following equation has usually been used to estimate their energy gaps:

$$\alpha h\nu = \left(h\nu - E_g\right)^n, \quad (1)$$

where α, h, ν, and E_g are the photonic absorbance, the Planck constant, photon frequency, and energy gap, respectively. The parameter n is a constant associated with different types of electronic transition: n = 1/2, 2, 3/2, or 3 for direct allowed, indirect allowed, direct forbidden, and indirect forbidden transitions, respectively, [9, 12, 21, 24]. UV-visible spectra (Figure 9) of α-MoO_3 and h-MoO_3 show a photonic energy attenuated through the solids. The $(\alpha h\nu)^2$ versus $h\nu$ plots were used to estimate energy gaps of α-MoO_3 and h-MoO_3 to be 3.18 and 3.05 eV, respectively. These energy gaps are in accordance with those of 3.35 eV for polycrystalline α-MoO_3 thin film [12], 3.75 eV α-MoO_3 nanobelts [9], 3.15 eV for α-MoO_3 layered structure and 3.01 eV for h-MoO_3 hexagonal rods [15], and 2.99 eV for h-MoO_3 hexagonal nanorods [16]. Shape, size, size distribution, phase, crystalline degree, and defects can play a role in the energy gaps of materials. Generally, E_g becomes wider by using smaller particles but narrower by the presence of defects.

4. Conclusions

In this research, h-MoO_3 rods with the shape of flowers were successfully synthesized by refluxing process and further calcination of the flower-like product to form α-MoO_3 microplates. Their phases, morphologies, and vibration modes were characterized by XRD, SEM, TEM, SAED, and FTIR. Degradation of MB dye under xenon light was proceeding by the photocatalysis and photosensitization processes. Catalytic activity of the metastable h-MoO_3 phase has higher efficiency than that of the thermodynamically stable α-MoO_3 one. PL emissions were determined to be 436 nm for α-MoO_3 microplates, and 436 and 606 nm for h-MoO_3 rods, including E_g of 3.18 eV for α-MoO_3 microplates, and 3.05 eV for h-MoO_3 rods. Their phase and morphology transformation was also explained according to the experimental results.

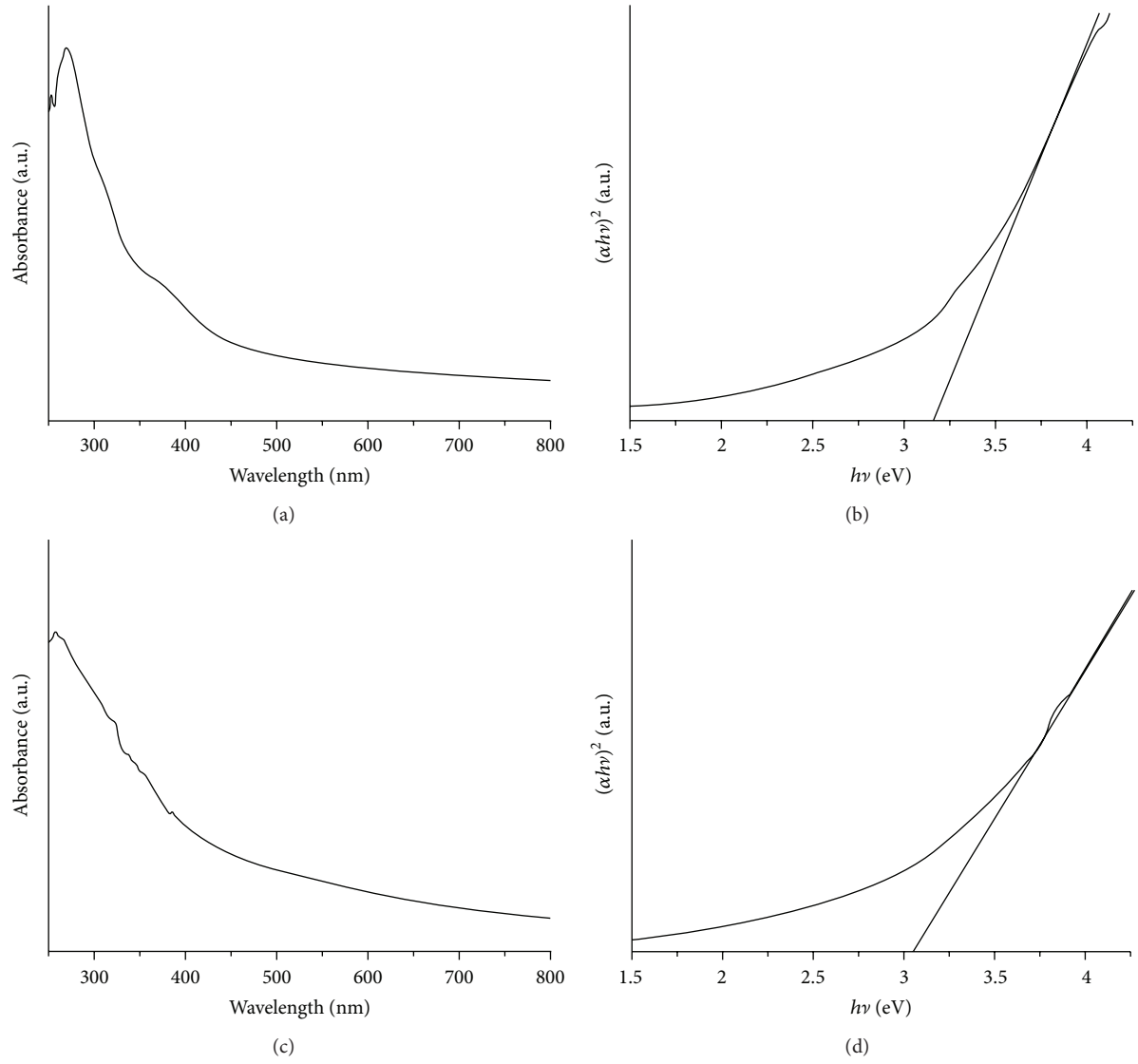

FIGURE 9: UV-visible absorbance and the $(\alpha h\nu)^2$ versus $h\nu$ plots of ((a), (b)) α-MoO_3 and ((c), (d)) h-MoO_3.

Acknowledgments

The authors wish to thank the National Nanotechnology Center (NANOTEC), National Science and Technology Development Agency (NSTDA), for providing financial support through Project P-10-11345, the Thailand's Office of the Higher Education Commission through the National Research University (NRU) Project for Chiang Mai University (CMU), the National Research Council of Thailand (NRCT) through the research project for fiscal year 2556, and the Center for Innovation in Chemistry (PERCH-CIC), including the Graduate School of CMU through a general support.

References

[1] S. Deki, A. B. Béléké, Y. Kotani, and M. Mizuhata, "Liquid phase deposition synthesis of hexagonal molybdenum trioxide thin films," *Journal of Solid State Chemistry*, vol. 182, no. 9, pp. 2362–2367, 2009.

[2] T. He, Y. Ma, Y. Cao, Y. Yin, W. Yang, and J. Yao, "Enhanced visible-light coloration and its mechanism of MoO_3 thin films by Au nanoparticles," *Applied Surface Science*, vol. 180, no. 3-4, pp. 336–340, 2001.

[3] K. Du, W. Fu, R. Wei et al., "Ultrasonic-assisted synthesis of highly dispersed MoO_3 nanospheres using 3-mercaptopropyltrimethoxysilane," *Ultrasonics Sonochemistry*, vol. 15, no. 3, pp. 233–238, 2008.

[4] J. Song, X. Ni, L. Gao, and H. Zheng, "Synthesis of metastable h-MoO_3 by simple chemical precipitation," *Materials Chemistry and Physics*, vol. 102, no. 2-3, pp. 245–248, 2007.

[5] S. Bai, S. Chen, L. Chen et al., "Ultrasonic synthesis of MoO_3 nanorods and their gas sensing properties," *Sensors and Actuators B*, vol. 174, pp. 51–58, 2012.

[6] Z. Wu, D. Wang, X. Liang, and A. Sun, "Ultrasonic-assisted preparation of metastable hexagonal MoO_3 nanorods and their

transformation to microbelts," *Ultrasonics Sonochemistry*, vol. 18, no. 1, pp. 288–292, 2011.

[7] S. R. Dhage, M. S. Hassan, and O.-B. Yang, "Low temperature fabrication of hexagon shaped h-MoO_3 nanorods and its phase transformation," *Materials Chemistry and Physics*, vol. 114, no. 2-3, pp. 511–514, 2009.

[8] B. Gao, H. Fan, and X. Zhang, "Hydrothermal synthesis of single crystal MoO_3 nanobelts and their electrochemical properties as cathode electrode materials for rechargeable lithium batteries," *Journal of Physics and Chemistry of Solids*, vol. 73, no. 3, pp. 423–429, 2012.

[9] H. Sinaim, D. J. Ham, J. S. Lee, A. Phuruangrat, S. Thongtem, and T. Thongtem, "Free-polymer controlling morphology of α-MoO_3 nanobelts by a facile hydrothermal synthesis, their electrochemistry for hydrogen evolution reactions and optical properties," *Journal of Alloys and Compounds*, vol. 516, pp. 172–178, 2012.

[10] J. Song, X. Ni, D. Zhang, and H. Zheng, "Fabrication and photoluminescence properties of hexagonal MoO_3 rods," *Solid State Sciences*, vol. 8, no. 10, pp. 1164–1167, 2006.

[11] D. Parviz, M. Kazemeini, A. M. Rashidi, and K. Jafari Jozani, "Synthesis and characterization of MoO_3 nanostructures by solution combustion method employing morphology and size control," *Journal of Nanoparticle Research*, vol. 12, no. 4, pp. 1509–1521, 2010.

[12] L. Boudaoud, N. Benramdane, R. Desfeux, B. Khelifa, and C. Mathieu, "Structural and optical properties of MoO_3 and V_2O_5 thin films prepared by Spray Pyrolysis," *Catalysis Today*, vol. 113, no. 3-4, pp. 230–234, 2006.

[13] H. Sinaim, A. Phuruangrat, S. Thongtem, and T. Thongtem, "Synthesis and characterization of heteronanostructured Ag nanoparticles/MoO_3 nanobelts composites," *Materials Chemistry and Physics*, vol. 132, no. 2-3, pp. 358–363, 2012.

[14] Y. Chen, C. Lu, L. Xu, Y. Ma, W. Hou, and J. Zhu, "Single-crystalline orthorhombic molybdenum oxide nanobelts: synthesis and photocatalytic properties," *CrystEngComm*, vol. 12, no. 11, pp. 3740–3747, 2010.

[15] A. Chithambararaj and A. C. Bose, "Hydrothermal synthesis of hexagonal and orthorhombic MoO_3 nanoparticles," *Journal of Alloys and Compounds*, vol. 509, no. 31, pp. 8105–8110, 2011.

[16] A. Chithambararaj and A. C. Bose, "Investigation on structural, thermal, optical and sensing properties of meta-stable hexagonal MoO_3 nanocrystals of one dimensional structure," *Beilstein Journal of Nanotechnology*, vol. 2, no. 1, pp. 585–592, 2011.

[17] V. V. Atuchin, T. A. Gavrilova, V. G. Kostrovsky, L. D. Pokrovsky, and I. B. Troitskaia, "Morphology and structure of hexagonal MoO_3 nanorods," *Inorganic Materials*, vol. 44, no. 6, pp. 622–627, 2008.

[18] A. Klinbumrung, T. Thongtem, and S. Thongtem, "Characterization of orthorhombic α-MoO_3 microplates produced by a microwave plasma process," *Journal of Nanomaterials*, vol. 2012, Article ID 930763, 5 pages, 2012.

[19] L. X. Song, J. Xia, Z. Dang, J. Yang, L. B. Wang, and J. Chen, "Formation, structure and physical properties of a series of α-MoO_3 nanocrystals: from 3D to 1D and 2D," *CrystEngComm*, vol. 14, no. 8, pp. 2675–2682, 2012.

[20] Powder Diffract. File, JCPDS-ICDD, 12 Campus Boulevard, Newtown Square, PA 19073-3273, USA., 2001.

[21] J. Huang, C. Xia, L. Cao, and X. Zeng, "Facile microwave hydrothermal synthesis of zinc oxide one-dimensional nanostructure with three-dimensional morphology," *Materials Science and Engineering B*, vol. 150, no. 3, pp. 187–193, 2008.

[22] Y. Ku, Y. Huang, and Y. Chou, "Preparation and characterization of ZnO/TiO2 for the photocatalytic reduction of Cr(VI) in aqueous solution," *Journal of Molecular Catalysis A*, vol. 342-343, pp. 18–22, 2011.

[23] M. Vijay, V. Selvarajan, K. P. Sreekumar, J. Yu, S. Liu, and P. V. Ananthapadmanabhan, "Characterization and visible light photocatalytic properties of nanocrystalline TiO_2 synthesized by reactive plasma processing," *Solar Energy Materials and Solar Cells*, vol. 93, no. 9, pp. 1540–1549, 2009.

[24] R. Al-Gaashani, S. Radiman, Y. Al-Douri, N. Tabet, and A. R. Daud, "Investigation of the optical properties of $Mg(OH)_2$ and MgO nanostructures obtained by microwave-assisted methods," *Journal of Alloys and Compounds*, vol. 521, pp. 71–76, 2012.